Available online at www.sciencedirect.com

SCIENCE DIRECT®

Journal of Computational Physics 211 (2006) 638–658

JOURNAL OF COMPUTATIONAL PHYSICS

www.elsevier.com/locate/jcp

A new numerical approach for the simulation of the growth of inorganic nanoparticles

N.M. Morgan [a], C.G. Wells [a], M.J. Goodson [a], M. Kraft [a,*], W. Wagner [b]

[a] *Department of Chemical Engineering, University of Cambridge, Pembroke Street, Cambridge CB2 3RA, UK*
[b] *Weierstrass Institute for Applied Analysis and Stochastics Mohrenstraße 39, D-10117 Berlin, Germany*

Received 24 May 2004; received in revised form 11 April 2005; accepted 14 April 2005
Available online 2 August 2005

Abstract

In this paper we derive and test an extended mass-flow type stochastic particle algorithm for simulating the growth of nanoparticles that are formed in flames and reactors. The algorithm incorporates the effects of coagulation that dominates such systems, along with a particle source and surface growth. We simulate three different configurations for the creation of nanoparticles. The oxidation of SiH_4 to SiO_2 and $Fe(CO)_5$ to Fe_2O_3 in premixed $H_2/O_2/Ar$ flames were investigated under different initial concentrations of SiH_4 and $Fe(CO)_5$, respectively. In addition, the oxidation of $TiCl_4$ to TiO_2 in a plug-flow reactor was investigated. A simple reaction mechanism for the conversion of $Fe(CO)_5$ to Fe_2O_3 was suggested, based on prior experimental data along with estimated transport properties for the species considered in this system. The simulation results were compared to experimental data available in the literature.

Keywords: Nanoparticles; Laminar flames; Particle growth; Stochastic simulation

1. Introduction

In this paper we present a solution method for population balance models which describe the synthesis and the dynamics of inorganic nanoparticles. One important method of their production is the synthesis in flames and plug flow reactors. The models which describe this process can be divided into three parts: a particle source linked to the gas-phase rate of production, a surface growth term linked to the gas-phase concentration of a precursor species and the surface area of the particles, and a coagulation term with a rate determined by a coagulation kernel.

[*] Corresponding author. Tel.: +44 1223 762784; fax: +44 1223 334796.
E-mail addresses: mk306@cam.ac.uk, markus_kraft@cheng.cam.ac.uk (M. Kraft).

0021-9991/$ - see front matter © 2005 Elsevier Inc. All rights reserved.
doi:10.1016/j.jcp.2005.04.027

Nomenclature

A	pre-exponential factor in Arrhenius expression (various)
$A_{\rm D}$	area density (m^{-1})
a_x	surface area of a particle of size x (m^2)
C	concentration of precursor chemical (mol m^{-3})
$c(0,x)$, $c_0(x)$	initial concentration of particles (m^{-3})
$c(t,x)$	concentration of particles of size x at time t (m^{-3})
$c_{\rm tot}$	total error in solution (various)
$D_{\rm f}$	fractal dimension (–)
$E_{\rm A}$	activation energy (J/mol)
$I^{\rm inf}$	rate of particle inception (m^{-3} s^{-1})
$I^{\rm surf}$	rate of surface growth (m^{-2} s^{-1})
$K(x,x')$, $\hat{K}(x,x')$	Coagulation kernel (m^3 s^{-1})
$k_{\rm B}$	Boltzmann's constant (J K^{-1})
$k_{\rm g}$	gas oxidation rate constant (s^{-1})
$k_{\rm s}$	surface oxidation rate constant (m s^{-1})
$k_{\rm total}$	total rate constant of precursor oxidation (s^{-1})
L	number of independent runs of the simulation (–)
m	mass of particle (kg)
M_n	the nth moment of the distribution (various)
N	number of stochastic particles (–)
Q	mass flow rate per unit area (kg m^{-2} s^{-1})
t	time (s)
$t_{\rm stop}$	time at end of simulation (s)
V	velocity (m s^{-1})
x, y	dimensionless volume (v/v_0) (–)
ρ_n	density of reactor gas (kg m^{-3})
ρ_s	particle density (kg m^{-3})
0	at initial conditions (–)
n	denotes at point n (–)

There exist three main ways to simulate such systems: the method of moments [1], the sectional method [2] and stochastic particle methods [3–6]. The method of moments uses moment evolution equations for the system, which are then solved so giving the time evolution of various moments of the particle system. This method is fast and relatively simple to implement; however it cannot fully generate the particle size distribution (PSD) and introduces closure problems. For the resolution of the PSD we may use a sectional method. This is a finite element method which replaces the partial differential equations with a series of ordinary differential equations. It can be incorporated very efficiently into standard flame simulations, hence its rather wide-spread use.

Stochastic particle methods have been developed for some years. In 1972, Gillespie [7] used a stochastic model to simulate cloud droplet growth. More recently, Eibeck and Wagner [8–10] and Kolodko and Sabelfeld [11] applied such ideas to coagulation and fragmentation problems, deriving both the direct simulation algorithm (DSA) [12,13] and mass-flow algorithm (MFA) with their accompanying convergence proofs and exploiting majorant kernels for the reduction of the complexity of the algorithm. These methods have been applied to chemical engineering by Goodson and Kraft [14] who studied the convergence properties of their algorithm and by Grosschmidt et al. [5] who applied such an algorithm to simulate the production of silica. A similar extension to the model, subsequently solved by a stochastic MFA has been performed by Debry et al. [15]. However, there are a number of differences between their algorithm and the one used in [5]. In [15] they make use of a deterministic time step equal to the maximum value of a majorized coagulation kernel, but do not discuss the introduction of fictitious jumps. They also use operator splitting methods to simulate processes other than coagulation and make use of a bin method for particle storage and selection. Their algorithm scales with time as $N^{3/2}$ rather than linearly with N as demonstrated in [14] where N is a measure of the number of stochastic particles.

In this paper, we present an extension of the MFA [10,16] that generates a solution to Smoluchowski coagulation equation with surface growth and a particle source. The algorithm presented in this paper is used to calculate an exponentially distributed time step based on a majorant kernel and introduces fictitious jumps to compensate for the use of the majorant, uses stochastic jumps for all processes and makes use of a binary tree method for the determination of the coagulation partners. The algorithm presented in this paper is derived from first principles from the original equation stated.

The results of a computational implementation of this algorithm are then compared to similar results from the DSA to study its convergence properties and physical systems for which experimental measurements have been obtained. We apply this algorithm to the production of titania. In this system, the surface reaction rate and the gas phase oxidation rate are not independent; however the algorithm can be altered to allow for systems where there is no interdependance.

2. Coupling the flame simulations to the population balance model

In order to simulate a 1D inhomogeneous flame-particle system, first the associated flame equations for the gas-phase must be solved. The flame equations [17] describe the evolution of the various species created and destroyed in the flame and include convection and diffusion along with other mechanisms. We solve the flame equations using the 1D flame code, PREMIX [18]. PREMIX solves the equations using a damped form of Newton's method. For the stochastic simulation, we require three pieces of information from the solution to the flame model: the velocity field, the temperature profile and the rate of production of the particulate species along the length of the axis.

It is important to mention at this point that our population balance model is spatially homogeneous in nature. As such, what is simulated is a Lagrangian view of particles in a control volume that moves with the velocity field. We assume that no particles leave the control volume up or down stream and that mass can only enter the volume from the gas phase production of the desired species from the particle source or surface growth.

In order to use the results from the PREMIX code in the stochastic coagulation code, it is necessary to convert the independent variable from a spatial coordinate to a time coordinate which will be used as the residence time of the particles. It is straightforward to calculate the velocity, V, of the flow field at any of the PREMIX calculated points, n, using the flow rate that PREMIX outputs, Q and density, ρ. Note that as PREMIX is a 1D simulation package, Q has units of kg m^{-2} s^{-1}.

$$V_n = \frac{Q_n}{\rho_n}. \tag{1}$$

The time, t_n, is then calculated from the average speed between points i and $i-1$ and the distance between these points

$$t_n = 2\sum_{i=1}^{n} \frac{x_i - x_{i-1}}{V_i + V_{i-1}}, \quad t_0 = 0. \tag{2}$$

This is the same as numerically integrating 1/velocity with respect to distance using a simple trapezium rule.

The temperature and rate of production of the particle species can now be written in terms of time and used for the population balance model.

3. Population balance model

The model we construct for the growth of nanoparticles in flames contains three different processes: a particle source, surface growth and coagulation. The governing equation, extending the Smoluchowski coagulation equation [19], is given below

$$\frac{\partial}{\partial t}c(t,x) = \frac{1}{2}\sum_{y=1}^{x-1}K(x-y,y)c(t,x-y)c(t,y) - \sum_{y=1}^{\infty}K(x,y)c(t,x)c(t,y) + I^{\text{inf}}c^{\text{in}}(x) + I^{\text{surf}}[a_{x-1}c(t,x-1) - a_x c(t,x)], \tag{3}$$

where $c(t,x)$ is the concentration of particles of size x (where x is a dimensionless volume $= v/v_0$), at time t, subject to the initial condition

$$c(0,x) = c_0(x) \geqslant 0. \tag{4}$$

The sections which follow describe the terms in Eq. (3).

3.1. Particle source

New mass is allowed to enter the particle system as monomeric particles produced from the gas phase. The equation that describes the time evolution of this process is shown below

$$\frac{\partial}{\partial t}c(t,x) = I^{\text{inf}}c^{\text{in}}(x), \tag{5}$$

where c^{in} describes a source of particles of unit size (with mass m_0, volume v_0, surface area a_0 and radius r_0)

$$c^{\text{in}}(x) = \delta(1,x), \tag{6}$$

where δ is the Kronecker delta and the rate of production, I^{inf}, is the gas phase rate of production of these monomers.

3.2. Surface growth

Some particle systems, for example $TiCl_4 + O_2 \rightarrow TiO_2 + 2Cl_2$, allow growth through the deposition of new mass directly onto the surface of an existing particle. In certain circumstances, it makes a significant contribution to the growth of particles and thus should be included in a simulation [20]. The size evolution of particles due to surface growth can be described by

$$\frac{\partial}{\partial t}c(t,x) = I^{\text{surf}}[a_{x-1}c(t,x-1) - a_x c(t,x)], \tag{7}$$

where I^{surf} is the overall rate of deposition of mass onto the surface of all particles in the system and a_x is the surface area of a particle of size x. In this model, we consider the deposition of monomeric particles onto the surface of existing particles, thus taking them from a volume of $v - v_0$ to v and area $a - a_0$ to a. Eq. (7) therefore describes the rate of change of particles from size $x - 1$ up to size x and is proportional to the surface area and concentration of the particles.

In the case of TiO_2 it is possible to approximate the system by one reaction as opposed to a set of coupled reactions. The reaction of $TiCl_4 + O_2 \rightarrow TiO_2 + 2Cl_2$ has an overall observed rate such that the rate of change of $TiCl_4$ concentration is [21]

$$\frac{\mathrm{d}C}{\mathrm{d}t} = -k_{\mathrm{total}}C, \tag{8}$$

where C is the concentration of $TiCl_4$ remaining in the system and k_{total} is the rate constant. The parameter k_{total} is made up of two competing mechanisms; one which reacts $TiCl_4$ with O_2 to form monomers of TiO_2 and has an associated rate constant of k_{g} and another process which tries to react $TiCl_4$ on the surface of an oxide particle (and hence is termed surface growth), with an associated rate of $k_{\mathrm{s}}A_{\mathrm{D}}$. Here A_{D} is the area density of the system (i.e., the total surface area of the particles divided by the control volume they are contained in). The two rates are related through the overall rate constant thus

$$k_{\mathrm{total}} = k_{\mathrm{g}} + k_{\mathrm{s}}A_{\mathrm{D}}. \tag{9}$$

The total amount of $TiCl_4$ removed from the system remains the same whether surface growth is included or not. The reacted $TiCl_4$ is then split between surface growth and particle inception with the rates being

$$I^{\mathrm{inf}} = k_{\mathrm{g}}CN_{\mathrm{A}}\ [\mathrm{m}^{-3}\ \mathrm{s}^{-1}], \quad \text{and} \quad I^{\mathrm{surf}} = k_{\mathrm{s}}CN_{\mathrm{A}}\ [\mathrm{m}^{-2}\ \mathrm{s}^{-1}], \tag{10}$$

where N_{A} is Avogadro's constant. Note that k_{g} is calculated from prior knowledge of k_{total} and k_{s} by rearranging Eq. (9).

In order to implement this algorithm we must calculate the surface area, a, from the volume. At this point in the paper, it is prudent to have a small discussion about the nature of the particles that we are simulating. Sintering (that is to say the coalescence of particles into spherical 'primary' particles) is a very important mechanism, however in this simple model with only one internal coordinate, we do not consider it as a separate mechanism. As such, and in order to take account of this process, we will assume that the particles in the system instantaneously partially-sinter such that their surface area is reduced by some small amount. This amount is determined by the constant fractal dimension chosen for the simulation. We assume that the particles have a constant fractal dimension, D_{f}, defined by [22]

$$\frac{v}{v_0} = \left(\frac{r}{r_0}\right)^{D_{\mathrm{f}}} = \left(\frac{a}{a_0}\right)^{D_{\mathrm{f}}/2}. \tag{11}$$

If we assume that the smallest particle is spherical, then a_0 is calculated by

$$a_0 = 4\pi\left(\frac{3m_0}{4\pi\rho_s}\right)^{2/3} \tag{12}$$

and hence we can calculate the surface area from

$$a = a_0\left(\frac{v}{v_0}\right)^{2/D_{\mathrm{f}}} = a_0x^{2/D_{\mathrm{f}}}. \tag{13}$$

Values can range from 2.0 to 3.0, where $D_{\mathrm{f}} = 2.0$ would denote unsintered aggregates and $D_{\mathrm{f}} = 3.0$ fully coalesced spheres.

3.3. Coagulation model

Coagulation of particles is modelled using Smoluchowski's coagulation equation [19] with a kernel suitable for the flames simulated

$$\frac{\partial}{\partial t}c(t,x) = \frac{1}{2}\sum_{y=1}^{x-1}K(x-y,y)c(t,x-y)c(t,y) - \sum_{y=1}^{\infty}K(x,y)c(t,x)c(t,y). \tag{14}$$

The first term in Eq. (14) describes the increase in concentration of particles of size x due to the coagulation of two smaller particles whose size sum to x. The second term describes the decrease in the concentration of particles of size x that occurs whenever a particle of size x coagulates with any other particle. These two operators describe the coagulation behaviour of the system.

The kernel used in this investigation is for coagulation occurring in the free-molecular regime. This is applicable when the mean free path of a particle is considerably greater than its effective diameter. The rate of coagulation of any two particles in the free-molecular regime is [14]

$$K(x,y) = \underbrace{\left(\frac{3}{4\pi}\right)^{\frac{2}{3}}\left(\frac{8\pi k_\mathrm{B}T}{\rho_s}\right)^{\frac{1}{2}}\left(\frac{m_0}{\rho_s}\right)^{\frac{1}{6}}}_{\alpha}\underbrace{\left(\frac{1}{x}+\frac{1}{y}\right)^{\frac{1}{2}}\left(x^{\frac{1}{D_\mathrm{f}}}+y^{\frac{1}{D_\mathrm{f}}}\right)^{2}}_{\beta(x,y)}, \tag{15}$$

where α can be thought of as the scaling factor of the kernel and $\beta(x,y)$ is a dimensionless kernel. In the scaling factor, k_B is Boltzmann's constant, T is the temperature and ρ_s is the particle density. The first factor on the right-hand side of Eq. (15) denotes terms for calculating the cross sectional area of the particles, the second factor comes from kinetic theory of gases and is related to the relative speeds of any two particles and the third factor comes from the calculation of both the mass and areas of the particles.

4. Solving the population balance model

4.1. Deriving the mass-flow vague form

In this section, we introduce the mass-flow vague form of the extended Smoluchowski equation. From this we are able to choose the generators of the stochastic process.

Starting with the integral form of Eq. (3)

$$\begin{aligned}\frac{\partial}{\partial t}c(t,x) &= \frac{1}{2}\int_0^x K(x-y,y)c(t,x-y)c(t,y)\,\mathrm{d}y - \int_0^\infty K(x,y)c(t,x)c(t,y)\,\mathrm{d}y + I^{\mathrm{inf}}c^{\mathrm{in}}(x)\\ &\quad + I^{\mathrm{surf}}[a_{x-1}c(t,x-1) - a_x c(t,x)],\end{aligned} \tag{16}$$

we will be able to derive and deduce a set of stochastic generators for the processes in the population balance model. The equation is now multiplied by a continuous, compactly-supported test function, $\phi(x)$ and integrated over all x

$$\begin{aligned}\frac{\partial}{\partial t}\int_0^\infty \phi(x)c(t,x)\,\mathrm{d}x &= \int_0^\infty \phi(x)I^{\mathrm{inf}}c^{\mathrm{in}}(x)\,\mathrm{d}x + \int_0^\infty \phi(x)I^{\mathrm{surf}}a_0(x-1)^{2/D_\mathrm{f}}c(t,x-1)\,\mathrm{d}x\\ &\quad - \int_0^\infty \phi(x)I^{\mathrm{surf}}a_0x^{2/D_\mathrm{f}}c(t,x)\,\mathrm{d}x + \frac{1}{2}\int_0^\infty \phi(x)\\ &\quad \times \int_0^x K(x-y,y)c(t,x-y)c(t,y)\,\mathrm{d}y\,\mathrm{d}x\\ &\quad - \int_0^\infty \phi(x)\int_0^\infty K(x,y)c(t,x)c(t,y)\,\mathrm{d}y\,\mathrm{d}x.\end{aligned} \tag{17}$$

In order to get the equation into a form that allows generators to be easily extracted, certain substitutions can be made. The variable x in the first surface growth term is substituted for another variable, $y = x - 1$, yielding,

$$\int_0^\infty \phi(y+1)I^{\mathrm{surf}}a_0y^{2/D_\mathrm{f}}c(t,y)\,\mathrm{d}y - \int_0^\infty \phi(x)I^{\mathrm{surf}}a_0x^{2/D_\mathrm{f}}c(t,x)\,\mathrm{d}x. \tag{18}$$

In consequence the above equation may be written as

$$\int_0^\infty [\phi(x+1) - \phi(x)] I^{\mathrm{surf}} a_0 x^{2/D_{\mathrm{f}}} c(t,x)\, \mathrm{d}x. \tag{19}$$

Now, using the identity

$$\int_0^\infty \int_0^\infty \Psi(x,y)\, \mathrm{d}y\, \mathrm{d}x = \int_0^\infty \int_0^x \Psi(x-y,y)\, \mathrm{d}y\, \mathrm{d}x, \tag{20}$$

we can rewrite the last two terms of Eq. (17) as

$$\int_0^\infty \int_0^\infty \left[\frac{1}{2}\phi(x+y) - \phi(x)\right] K(x,y) c(t,x) c(t,y)\, \mathrm{d}y\, \mathrm{d}x. \tag{21}$$

Combining Eqs. (19) and (21) with Eq. (17) and allowing P to be a measure-valued solution of the equation such that

$$P(t,\mathrm{d}x) = c(t,x)\, \mathrm{d}x \tag{22}$$

and using the inner product defined by

$$\langle \phi, P(t) \rangle = \int_{\mathbb{N}} \phi(x) P(t,\mathrm{d}x), \tag{23}$$

we obtain

$$\begin{aligned} \frac{\partial}{\partial t}\langle \phi, P(t) \rangle = {} & \int_{\mathbb{N}} \phi(x) I^{\mathrm{inf}} P^{\mathrm{in}}(t,\mathrm{d}x) + \int_{\mathbb{N}} [\phi(x+1) - \phi(x)] I^{\mathrm{surf}} a_0 x^{2/D_{\mathrm{f}}} P(t,\mathrm{d}x) \\ & + \int_{\mathbb{N}^2} \left[\frac{1}{2}\phi(x+y) - \phi(x)\right] K(x,y) P(t,\mathrm{d}x) P(t,\mathrm{d}y), \end{aligned} \tag{24}$$

with $P_0(\mathrm{d}x) = P(0,\mathrm{d}x) = c(0,x)\, \mathrm{d}x$. The total mass of the system is calculated by

$$\int_{\mathbb{N}} x P(t,\mathrm{d}x). \tag{25}$$

We now call the measure,

$$Q(t,\mathrm{d}x) = x P(t,\mathrm{d}x), \quad t \geqslant 0, \tag{26}$$

the mass density and introduce a new continuous compactly-supported test function, $\psi(x)$, such that $x\psi(x) = \phi(x)$. Substituting into Eq. (24) we derive the mass flow equation

$$\begin{aligned} \frac{\partial}{\partial t}\langle \psi, Q(t) \rangle = {} & \int_{\mathbb{N}} \psi(x) I^{\mathrm{inf}} Q^{\mathrm{in}}(t,\mathrm{d}x) + \int_{\mathbb{N}} [(x+1)\psi(x+1) - x\psi(x)] I^{\mathrm{surf}} a_0 x^{2/D_{\mathrm{f}}} \frac{Q(t,\mathrm{d}x)}{x} \\ & + \int_{\mathbb{N}^2} [\psi(x+y) - \psi(x)] \frac{K(x,y)}{y} Q(t,\mathrm{d}x) Q(t,\mathrm{d}y), \end{aligned} \tag{27}$$

where $Q_0(\mathrm{d}x) = Q(0,\mathrm{d}x) = xP(0,\mathrm{d}x)$.

4.2. Deriving the stochastic generators

In order to solve Eq. (27) we introduce a sequence of random variables that are measure-valued jump processes $Q_t^{(N)} \in \{\lambda \sum_{i=1}^{N} \delta_{x_i} | \lambda \in \mathbb{R},\ x_i \in \mathbb{N}\}$, such that there is weak convergence in distribution to Q as $N \to \infty$. We now let

$$Q_t^{(N)} = \lambda_t^{(N)} R_t^{(N)}. \tag{28}$$

Accordingly set

$$R_t^{(N)} = \sum_{i=1}^{N} \delta(x_i) \quad \text{and} \quad \lambda_t^{(N)} = \lambda_0^{(N)} \left(\frac{N}{N-1}\right)^{\alpha_t^{(N)}}. \tag{29}$$

For notational convenience in what follows we will drop the superscript $^{(N)}$.

The measure R represents a set of stochastic particles and λ_t an overall scaling factor. The parameter λ_0 is calculated from the initial concentration of particles in the system $c_0(x)$ by

$$\lambda_0 = \frac{c_0(x)}{N}. \tag{30}$$

Let $\Psi(\alpha, R)$ be a bounded measurable function. We will now consider

$$\frac{\partial}{\partial t}\Psi(\alpha, R) = G_\mathrm{i}^N \Psi(\alpha, R) + G_\mathrm{s}^N \Psi(\alpha, R) + G_\mathrm{c}^N \Psi(\alpha, R), \tag{31}$$

where $G_\mathrm{i}^N, G_\mathrm{s}^N$ and G_c^N are stochastic generators for particle inception, surface growth and coagulation, respectively. Matching terms from Eq. (31) with terms in Eq. (27) allows us to write down forms for the generators.

First we define the jump processes:

For coagulation

$$J_\mathrm{c}(\alpha, R, x, y) = (\alpha, R + \delta_{x+y} - \delta_x), \tag{32}$$

for particle inception

$$J_i(\alpha, R, y) = (\alpha + 1, R + \delta_1 - \delta_y) \tag{33}$$

and for surface growth

$$J_{s_1}(\alpha, R, x) = (\alpha, R + \delta_{x+1} - \delta_x) \tag{34}$$

and

$$J_{s_2}(\alpha, R, x, y) = (\alpha + 1, R + \delta_{x+1} - \delta_y). \tag{35}$$

We then use these jumps to define a set of generators:

For coagulation

$$G_\mathrm{c}^N \Psi(\alpha, R) = \lambda_0 \left(\frac{N}{N-1}\right)^{\alpha} \int_{\mathbb{N}^2} [\Psi(J_\mathrm{c}(\alpha, R, x, y) - \Psi(\alpha, R)] \frac{K(x, y)}{y} R(\mathrm{d}x) R(\mathrm{d}y), \tag{36}$$

for particle inception

$$G_i^N \Psi(\alpha, R) = \frac{I^\mathrm{inf}}{\lambda_0} \left(\frac{N-1}{N}\right)^{\alpha+1} \int_{\mathbb{N}} [\Psi(J_i(\alpha, R, y)) - \Psi(\alpha, R)] \frac{R(\mathrm{d}y)}{N}, \tag{37}$$

and for surface growth

$$\begin{aligned} G_\mathrm{s}^N \Psi(\alpha, R) = {} & I^\mathrm{surf} a_0 \int_{\mathbb{N}} x^{2/D_\mathrm{f}} [\Psi(J_{s_1}(\alpha, R, x)) - \Psi(\alpha, R)] R(\mathrm{d}x) + \frac{N-1}{N} I^\mathrm{surf} a_0 \int_{\mathbb{N}^2} x^{2/D_\mathrm{f}-1} [\Psi(J_{s_2}(\alpha, R, x, y)) \\ & - \Psi(\alpha, R)] R(\mathrm{d}x) \frac{R(\mathrm{d}y)}{N}. \end{aligned} \tag{38}$$

If we take $\Psi(\alpha, R)$ to be

$$\Psi(\alpha, R) = \lambda_0 \int_{\mathbb{N}} \left(\frac{N}{N-1}\right)^{\alpha} R(\mathrm{d}x)\psi(x) = \int_{\mathbb{N}} Q(\mathrm{d}x)\psi(x), \tag{39}$$

we find that:

For coagulation

$$G_{\mathrm{c}}^{N}\Psi(\alpha, R) = \lambda_0^2 \left(\frac{N}{N-1}\right)^{2\alpha} \int_{\mathbb{N}^2} [\psi(x+y) - \psi(x)] \frac{K(x,y)}{y} R(\mathrm{d}x)R(\mathrm{d}y), \tag{40}$$

for particle inception

$$G_{\mathrm{i}}^{N}\Psi(\alpha, R) = \lambda I^{\mathrm{inf}} \int_{\mathbb{N}} \psi(x)R^{\mathrm{in}}(t, \mathrm{d}x) = I^{\mathrm{inf}}\psi(1), \tag{41}$$

and for surface growth

$$G_{\mathrm{s}}^{N}\Psi(\alpha, R) = I^{\mathrm{surf}} a_0 \lambda_0 \left(\frac{N}{N-1}\right)^{\alpha} \int_{\mathbb{N}} x^{2/D_{\mathrm{f}}} \left[\left(1 + \frac{1}{x}\right)\psi(x+1) - x\psi(x)\right] R(\mathrm{d}x). \tag{42}$$

If we combine Eqs. (40)–(42) we obtain Eq. (27), showing that the choice of generators and jumps is consistent.

4.3. An algorithm for the simulation of nanoparticles with surface growth and source term

In this section, we describe a stochastic mass-flow algorithm. For a particle system $x_1, \ldots, x_N$, Eqs. (32)–(42) describe how and when these particles interact either with each other or the surrounding gas phase. The principle works as follows. We generate an exponentially distributed time with parameter equal to the sum of all rates. After this time we let the particles interact. This interaction will be called a jump, motivated by the underlying jump-process. The nature of the interaction is determined by the probability of each possible physical process, which is a function of the current state of the system. The corresponding event is chosen probabilistically according to the rates of each process.

A majorant form of the coagulation kernel, $\hat{K}(x_i, x_j)$, will be introduced into the algorithm. This is done to change the way the double sum over all particle pairs in the coagulation generator is calculated. Instead of one double sum with complexity $\mathcal{O}(N^2)$ we calculate two independent sums and multiply them, reducing the complexity towards $\mathcal{O}(N)$. This introduces the concept of fictitious jumps where no jump is performed. Fictitious jumps occur with probability

$$1 - \frac{K(x_i, x_j)}{\hat{K}(x_i, x_j)} \tag{43}$$

and so we take care to choose the majorant such that we reduce the number that occur.

The algorithm is as follows:

(1) Generate initial state ($x_1, \ldots, x_N$, $\lambda = \lambda_0$, $\alpha = 0$) and choose t_{stop}

(2) Calculate the total area density, A_{D} from

$$A_{\mathrm{D}} = \lambda \sum_{i=1}^{N} \frac{a_i}{x_i} = \lambda a_0 \sum_{i=1}^{N} \frac{x_i^{2/D_{\mathrm{f}}}}{x_i} \tag{44}$$

and hence calculate k_{g} from Eq. (9).

(3) Generate an exponentially distributed time step τ, with parameter

$$\hat{\varrho}(p) = \hat{\varrho}_{\mathrm{c}}(p) + \varrho_{\mathrm{i}}(p) + \varrho_{S_1}(p) + \varrho_{S_2}(p), \tag{45}$$

$$\hat{\varrho}(p) = \lambda \sum_{i=1}^{N} \sum_{j=1}^{N} \frac{\hat{K}(x_i, x_j)}{x_j} + \frac{I^{\mathrm{inf}}}{\lambda} + I^{\mathrm{surf}} \sum_{i=1}^{N} a_0 x_i^{2/D_{\mathrm{f}}} + I^{\mathrm{surf}} \left(\frac{N-1}{N}\right) \sum_{i=1}^{N} a_0 x_i^{2/D_{\mathrm{f}}-1} \tag{46}$$

and increase time according to

$$t \mapsto t + \tau \tag{47}$$

if $t \geqslant t_{\mathrm{stop}}$ then stop the simulation, otherwise go to step 4.

(4) With probabilities

$$\frac{\varrho_{\mathrm{i}}(p)}{\hat{\varrho}(p)}, \frac{\varrho_{S_1}(p)}{\hat{\varrho}(p)}, \frac{\varrho_{S_2}(p)}{\hat{\varrho}(p)}, \frac{\hat{\varrho}_{\mathrm{c}}(p)}{\hat{\varrho}(p)} \tag{48}$$

go to step 5, 6, 7 or 8, respectively.

(5) Perform a particle inception step:
(a) Replace a uniformly chosen particle from the ensemble by a particle of size 1.
(b) $\alpha \mapsto \alpha + 1$.
(c) Return to step 2.

(6) Perform a surface growth step (type 1):
(a) Choose a particle, i, according to the distribution:

$$\frac{x_i^{2/D_{\mathrm{f}}}}{\sum_{k=1}^{N} x_k^{2/D_{\mathrm{f}}}}. \tag{49}$$

(b) Replace particle i and with a particle of size $x_i + 1$.
(c) Return to step 2.

(7) Perform a surface growth step (type 2):
(a) Choose a particle, i, according to the distribution

$$\frac{x_i^{2/D_{\mathrm{f}}-1}}{\sum_{k=1}^{N} x_k^{2/D_{\mathrm{f}}-1}} \tag{50}$$

and a particle j uniformly.
(b) Replace particle j with a particle of size $x_i + 1$.
(c) $\alpha \mapsto \alpha + 1$.
(d) Return to step 2.

(8) Perform a coagulation step:
(a) Choose particles i and j according to the distribution:

$$\frac{\frac{\hat{K}(x_i, x_j)}{x_j}}{\sum_{i,j} \frac{\hat{K}(x_j, x_j)}{x_j}}, \quad i \neq j. \tag{51}$$

(b) With probability

$$\frac{K(x_i, x_j)}{\hat{K}(x_i, x_j)} \tag{52}$$

add a particle of size $(x_i + x_j)$ to the particle ensemble and remove one of size x_i. Otherwise the jump is fictional and the particles do not interact.

(c) Return to step 2.

5. Numerical investigation of the mass-flow algorithm

5.1. The test simulation

A test case was used in order to study the convergence properties of the MFA compared to the DSA for speed and accuracy. The main macroscopic quantities we look at in this paper are the average mass and the first, second and third moments of the distribution. These functionals were chosen as in this rather limited analysis, quantities that would be of use in industrial applications (mean, standard deviation and skewness) were thought to be the most useful. As such this analysis is not to be taken as a complete convergence study, but an initial investigation into the algorithm's properties.

The parameters for the DSA test case were as follows:[1]

To study the systematic error of the algorithm, we use a reference solution which corresponds to the numerical solution obtained using one run at the largest feasible N.

In the mass-flow formulation, the average mass is proportional to the harmonic mean of the sizes $\{x_i\}$

$$m_0\left(\frac{1}{N}\sum_{i=1}^{N}x_i^{-1}\right)^{-1} \tag{53}$$

and in all following simulations, the average mass is calculated using this formula. Average diameters are calculated by converting the average mass to an equivalent diameter. The nth mass moment density is calculated by

$$\mathrm{M}n = \frac{c_0 m_0^n}{N}\left(\frac{N}{N-1}\right)^{\alpha}\sum_{i=1}^{N}x_i^{n-1}. \tag{54}$$

The moments of the distribution were determined and errors in the solutions at various different values of N were calculated in accordance with the methods used in [23].

In this investigation, the simulations were run for 8 h on a 1.2 GHz Athlon PC at each value of N, allowing as many runs within that time as could be performed. The input parameters were as in Table 1 with the exception of N (which varied from 128 to 16384) and L (which varied inversely with N). In this way the product $N \times L$ was kept approximately constant.

5.2. Results of the test simulation

The results for the CPU times and errors in the first three moments were as in Table 1. The parameters t_{sr} and c_{tot} being the CPU time for a single run and the total error, respectively.

One can see from Table 2 and Fig. 1 that the CPU time for the mass flow algorithm scales linearly with N. This is in agreement with the improved DSA investigated by Goodson and Kraft [14] and is a consequence of using a linearly majorant kernel for the coagulation calculations.

[1] These values are not physical for a real nanoparticle system, they have been chosen to represent a test case that can be simulated in a short time.

Table 1
Parameters for the test case

Description	Parameter	Value	Units
Kernel scaling factor	α	1.0	$m^3 s^{-1}$
Inflow rate (inception)	I^{inf}	0.5	$m^{-3} s^{-1}$
Fractal dimension	D_f	2.1	–
Number of particles	N	2097152	–
Number of runs	L	1	–
Initial concentration	$c_0(x)$	1.0	m^{-3}
Length of simulation	t_{stop}	5.0	s
Mass of monomer	m_0	1.0	kg
Volume of monomer	v_0	1.0	m^3

Table 2
CPU times and errors for algorithm

N	t_{sr} [s]	c_{tot} Ave. size	$\%c_{tot}$ Ave. size	$\%c_{tot}$ M2	$\%c_{tot}$ M3
128	0.39425	0.079237	0.96699	0.81405	2.1103
256	0.76793	0.038381	0.48252	0.43410	1.1106
512	1.5545	0.019825	0.23995	0.22174	0.56378
1024	3.1492	0.011917	0.13249	0.12075	0.29748
2048	6.4304	0.0080560	0.081518	0.085047	0.18720
4096	13.188	0.0056460	0.052420	0.068252	0.14136
8192	29.219	0.0047430	0.043318	0.051557	0.10644
16384	61.637	0.0039410	0.033091	0.046613	0.092308

The reduction of the total error in average size (Fig. 2) seems to fall as $1/\sqrt{N}$ as is expected from a Monte Carlo simulation. This is in contrast to the convergence properties reported in [14] which seems to indicate that the algorithm converges as $1/N$ throughout. The discrepancy here would seem to come from the way in which the investigation was carried out. In this paper, the investigation was run for 8 h as this

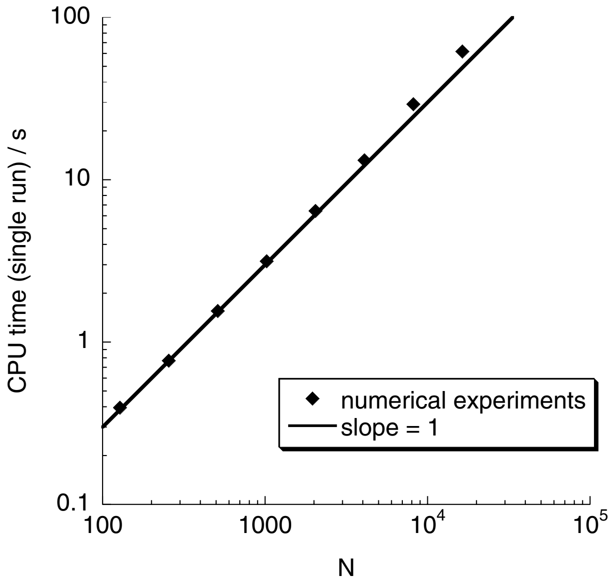

Fig. 1. CPU time for single runs at various values of N.

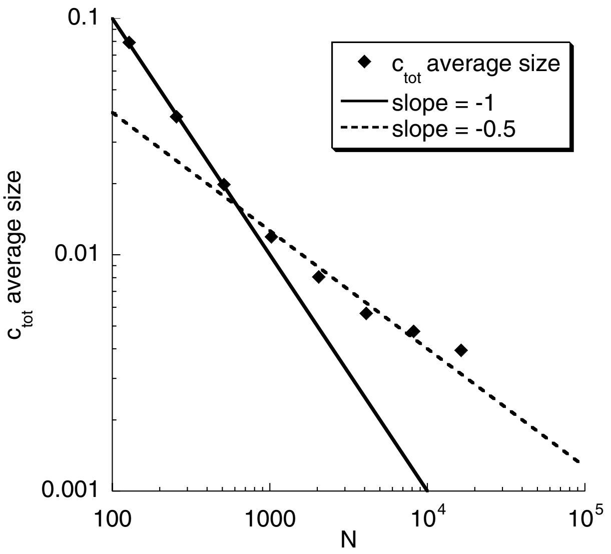

Fig. 2. Total error in average size vs *N*.

gave statistical errors in the solution of the same order of magnitude of those calculated in [14] (of approximately 0.07). In [14] this was sufficient to ensure that the statistical errors were considerably less than the systematic errors. Using the mass flow algorithm however, the initial systematic error was two orders of magnitude less than if the DSA had been used. As such the statistical error was larger than the systematic error and thus the order of convergence as defined in [23] and stated in [14] could not be calculated.

Fig. 3 shows the relative errors for average size and for the second and third moments of the distribution. As with the total error in average size, the errors in these quantities also decrease as $1/\sqrt{N}$.

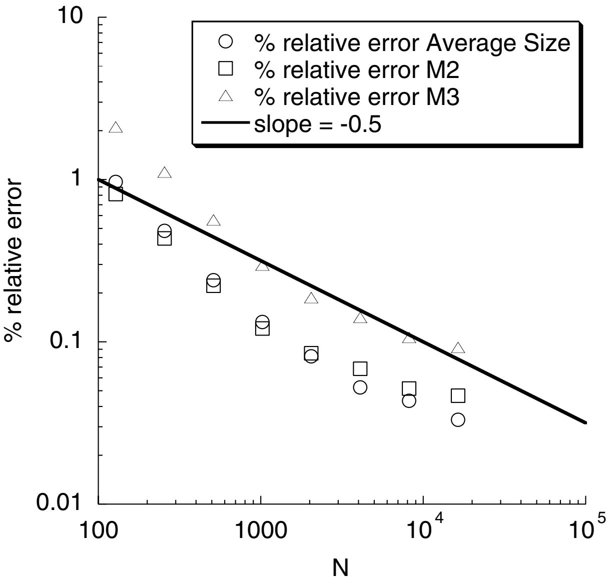

Fig. 3. Percentage relative error in average size, M2 and M3 vs *N*.

6. Simulated systems

Two of the three particle systems are simulated as low pressure $H_2/O_2/Ar$ flames doped with a precursor (SiH_4 or $Fe(CO)_5$ to generate particles of SiO_2 and Fe_2O_3, respectively). The third reaction scheme describes the oxidation of $TiCl_4$ to TiO_2 at atmospheric pressure in a simple plug-flow reactor.

6.1. Low pressure $H_2/O_2/Ar$ flame with SiH_4 precursor

The SiH_4 gas phase kinetics are described by a combined mechanism, which contains 18 $H_2/O_2/Ar$ reactions plus a further 26 reactions to describe the oxidation of SiH_4 to SiO_2 [24]. All thermodynamic and transport properties were found in the CHEMKIN [25] and TRANFIT [26] libraries, respectively. The flames in this section were simulated at low pressures (30 mbar) and at a velocity of 1.32 ms^{-1}.

The evolution of SiO_2 particles under varying input concentrations of SiH_4 was investigated. The concentration was varied between 131 and 524 ppm with all other input parameters held constant (Table 3). For the coagulation simulation, the particle number N was set to 1024 and the simulation results averaged over 50 runs. The fractal dimension of the silica particles, D_f, was set to be 2.23.

The CPU time for the 50 runs was 34.18 s.

Fig. 4 shows the result of the coagulation simulation. The simulation results agree well with the experimental measurements of Lindackers et al. [24], predicting the increase in average particle mass (calculated using Eq. (53)) with the initial concentration of SiH_4. This figure also contains results of a sectional method to solve the population balance equation. We can see that the two methods show reasonable agreement, however this can only be taken as a first step in fully validating the stochastic particle method as we have only compared average masses and not the full particle size distributions.

6.2. Low pressure $H_2/O_2/Ar$ flame with $Fe(CO)_5$ precursor

Previous investigations into simulating the coagulation of Fe_2O_3 particles have assumed instantaneous decomposition of the $Fe(CO)_5$ into Fe_2O_3 [27]. For our paper a simple skeletal mechanism is proposed. The following $Fe(CO)_5$ kinetics were estimated from the experiments of Giesen et al. [28] and Woiki et al. [29]:

$$\mathrm{Fe(CO)_5} \xrightarrow{k_1} \mathrm{FeCO} + 4\mathrm{CO} \tag{55}$$

$$\mathrm{FeCO} \xrightarrow{k_2} \mathrm{Fe} + \mathrm{CO} \tag{56}$$

$$4\mathrm{Fe} + 3\mathrm{O_2} \xrightarrow{k_3} 2\mathrm{Fe_2O_3} \tag{57}$$

The three rate constants were fit to an Arrhenius equation

$$k_f = A \exp\left(\frac{-E_A}{RT}\right), \tag{58}$$

with the coefficients for the three chemical equations shown in Table 4.

Table 3
Input parameters for SiH_4 to SiO_2 flame

Parameter	Value
Initial flame velocity	1.32 ms^{-1}
Pressure	30 mbar
H_2:O_2	1.69 mol:mol
Ar:($H_2 + O_2$)	1.36 mol:mol
SiH_4 concentration	131–524 ppm

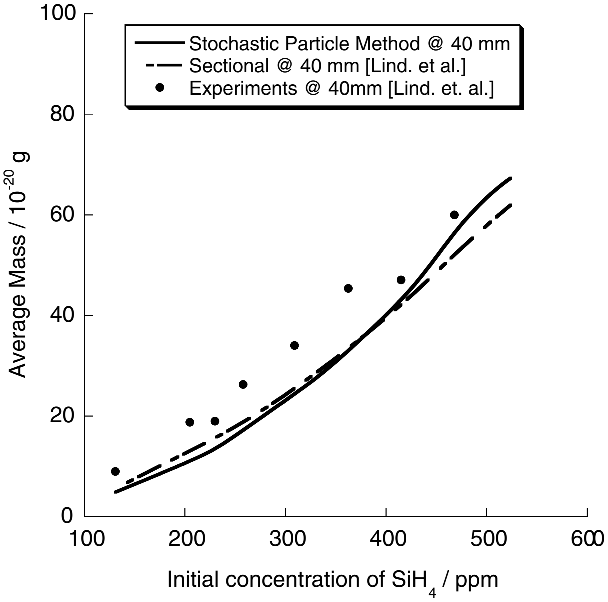

Fig. 4. Effect on average particle mass of initial concentration of SiH_4 precursor, simulation and experimental data. Measurements and simulations taken 40 mm from burner face.

Table 4
Rate constants for the proposed $Fe(CO)_5$ to Fe_2O_3 mechanism

	A [cm mol s]	E_A [J/mol]
k_1	4.00×10^9	72341.36
k_2	7.00×10^9	72341.36
k_3^*	7.00×10^{12}	0.0

Note that k_3 has been modified to k_3^* to allow for the reaction rate to be first order with respect to iron concentration and zeroth order with respect to oxygen concentration. The third reaction (Eq. (57)) is a much simplified form of the mechanism to account for the oxidation of Fe to Fe_2O_3. Its kinetics have been estimated in order to make that particular reaction faster than the other two reactions. We justify making this assumption as the paper by Janzen and Roth [27] assumes instant formation of Fe_2O_3 from $Fe(CO)_5$ at the start of the flame, whereas the paper by Giesen et al. [28] gives a finite rate for the decomposition of $Fe(CO)_5$. Since there is no further information about the rates, we chose to allow the oxidation part of the mechanism not to be the rate limiting step, hence its more rapid rate.

The transport properties of the Fe compounds were also estimated. This was done by comparing the molecules' size and shape to other species within the TRANFIT database and estimating values as required. The resulting TRANFIT constants are contained in Table 5.

The equations that use these constants can be found in the TRANFIT manual [26].

The evolution of Fe_2O_3 particles was investigated for a flame with initial conditions shown in Table 6. The coagulation simulation parameters were set to $N = 1024$, $L = 50$ and $D_f = 3.0$. The simulation took 35.28 s for the 50 runs.

Fig. 5 shows the result of the coagulation simulation. The evolution of the particle diameter (calculated using Eq. (11)) over time is in good agreement with the experimental data of Janzen et al. [27]. This result

Table 5
Estimated transport properties for Fe compounds

Species	C1	C2	C3	C4	C5	C6
Fe	0	2999.0	3.76	0.00	0.00	0.00
$Fe(CO)_5$	2	400.0	5.9	0.00	0.00	1.00
Fe(CO)	1	400.0	3.9	0.00	0.00	1.00
Fe_2O_3	2	400.0	4.5	0.00	0.00	1.00

The various constants are as follows:
C1 = shape constant where 0 = single atom, 1 = linear molecule, 2 = non-linear molecule.
C2 = the Lennard–Jones potential well depth ϵ/k_B [K].
C3 = the Lennard–Jones collision diameter σ [Å].
C4 = the dipole moment μ in Debye [10^{-18} $cm^{3/2}$ $erg^{1/2}$].
C5 = the polarizability α [$Å^3$].
C6 = the rotational relaxation collision number Z_{rot} at 298 K.

Table 6
Input parameters for $Fe(CO)_5$ to Fe_2O_3 flame

Parameter	Value
Initial flame velocity	1.32 ms^{-1}
Pressure	30 mbar
H_2:O_2	1.00 mol:mol
Ar:($H_2 + O_2$)	1.04 mol:mol
$Fe(CO)_5$ concentration	524 ppm

was obtained using a fractal dimension of 3.0, which implies that the particles sinter instantly to spherical particles.

The next set of simulations involved changing the initial concentration of $Fe(CO)_5$ between 262 and 1572 ppm whilst keeping all other variables constant. The parameters of the flame were as in Table 7. The simulation parameters for the coagulation were again $N = 1024$, $L = 50$ and $D_f = 3.0$. The simulations took between 30 and 50 s to complete.

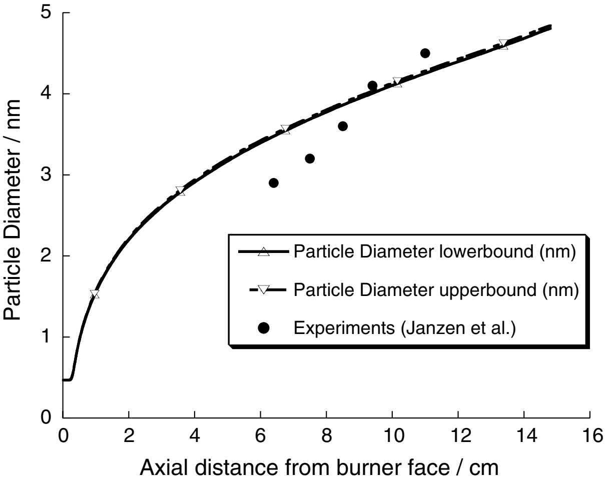

Fig. 5. Comparison of simulated particle size evolution vs experimental data. The lower bound and upper bound lines represent the limit of a 99.9% confidence interval of the empirical mean of the particle diameter.

Table 7
Input parameters for $Fe(CO)_5$ to Fe_2O_3 flames with varying initial concentrations of $Fe(CO)_5$

Parameter	Value
Initial flame velocity	1.32 ms^{-1}
Pressure	30 mbar
H_2:O_2	1.00 mol:mol
Ar:($H_2 + O_2$)	1.04 mol:mol
$Fe(CO)_5$ concentration	262–1572 ppm

Fig. 6 shows the results of the coagulation simulation. The illustrations and measurements show different trends, which seems odd especially when considering the excellent agreement that was obtained for the similar silica system. It is of note that the simulations carried out in [27] also over predict the particle diameters to a similar order of magnitude. We could attribute some of this discrepancy to a lack of kinetic data being available for the oxidation of $FeCO_5$ to Fe_2O_3. However it is more likely that we are simulating agglomeration type behaviour which would lead to a rapid growth in particle size, whereas the particle system is still at the primary particle growth stage. This behaviour illustrates one of the problems with neglecting particle sintering as a mechanism in the population balance.

6.3. $TiCl_4 \rightarrow TiO_2$ plug-flow reactor system

The final system simulated was the oxidation of $TiCl_4$ to form titania in a plug-flow reactor. Because this is a simple system, information about the kinetics of the reactions, the initial concentrations of reactants and the temperature profile of the reactor are sufficient for a simulation.

The oxidation of $TiCl_4$ to form TiO_2 is modelled as a single reaction

$$TiCl_4 + O_2 \xrightarrow{K} TiO_2 + 2Cl_2 \tag{59}$$

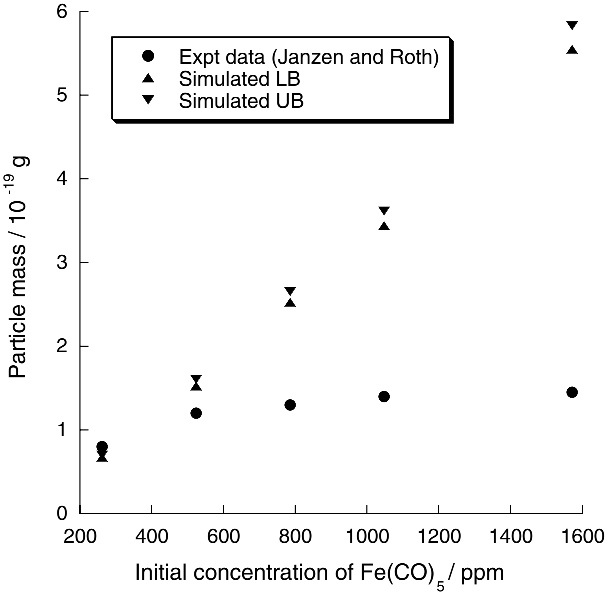

Fig. 6. Effect on average particle mass of initial concentration of $Fe(CO)_5$ precursor, simulation vs experimental data. The triangles mark the upper bound (UB) and lower bound (LB) of a 99.9% confidence interval for the empirical mean of the particle mass.

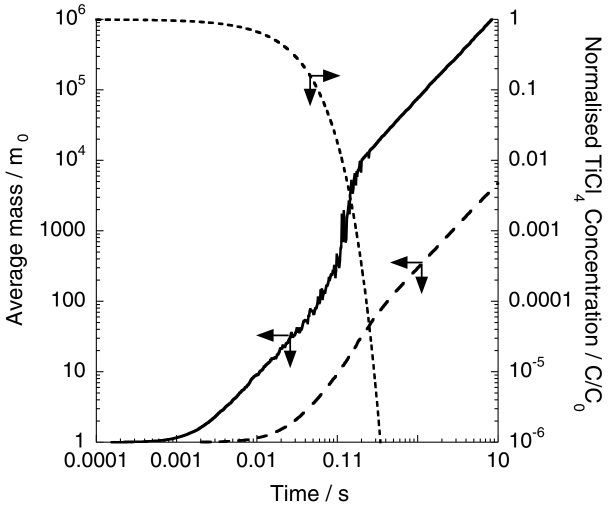

Fig. 7. Average mass of TiO_2 vs time. The solid line represents an initial mole fraction of $TiCl_4$ of 10^{-4} whilst the dashed line represents an initial mole fraction of 10^{-6}. The dotted line represents the normalized $TiCl_4$ concentration.

where K is the sum of the gas-phase and surface-growth rates as explained in Section 3.2. The kinetic data for this reaction is taken from the paper by Spicer et al. [20] whilst the thermodynamic data is taken from the NIST website [30]. No transport data are required.

First the system was simulated at 1400 K, with mole fractions of $TiCl_4$ of 10^{-4} and 10^{-6}. At these conditions and with 4096 stochastic particles, the simulations took little over 28 s per run.

Fig. 7 shows how the average particle mass increases over time. The extra mass speeds up the coagulation process and allows a rapid increase in average particle mass at around $t = 0.1$ s. This effect is due to the large particles in the system coagulating very rapidly with the new particles from the gas phase in accordance with the coagulation kernel. Once new particles cease to enter the system, the rate of the increase in particle mass becomes independent of the initial concentration of $TiCl_4$. This is to be expected and it is of note that this figure shows the same trends as shown in [21] for similar simulations.

The titania system was next simulated at a much higher initial concentration of $TiCl_4$ in order to make the effect of surface growth more noticeable. The temperature was again 1400 K but the initial mole fraction of $TiCl_4$ was now 1.0.

Fig. 8 shows various properties of the $TiCl_4$ system, simulated both with and without surface growth. In Fig. 8(a) we see that the average mass of the particles is larger when surface growth is included in the simulation compared to when we simulate particle inception and coagulation only. Fig. 8(b) shows that the same amount of mass is entering the system irrespective of whether there is surface growth or not. This shows that the addition of mass directly to a particle is more important than the increase in the concentration of particles for coagulation. Finally Fig. 8(c) shows the PSD at time $t = 0.001$ s of the systems.[2] We see that when surface growth is included in the simulation, a small additional peak is formed at around mass equals $8m_0$. This could correspond to small particles that normally would not form in large numbers through coagulation being formed via surface growth, however we should note that at this short time, only a very small amount of $TiCl_4$ has been converted to TiO_2 and thus further simulations will have to be run to investigate this further.

[2] The reader should note that as yet we have not been able to fully validate this distribution. As such it should only be viewed as illustrative.

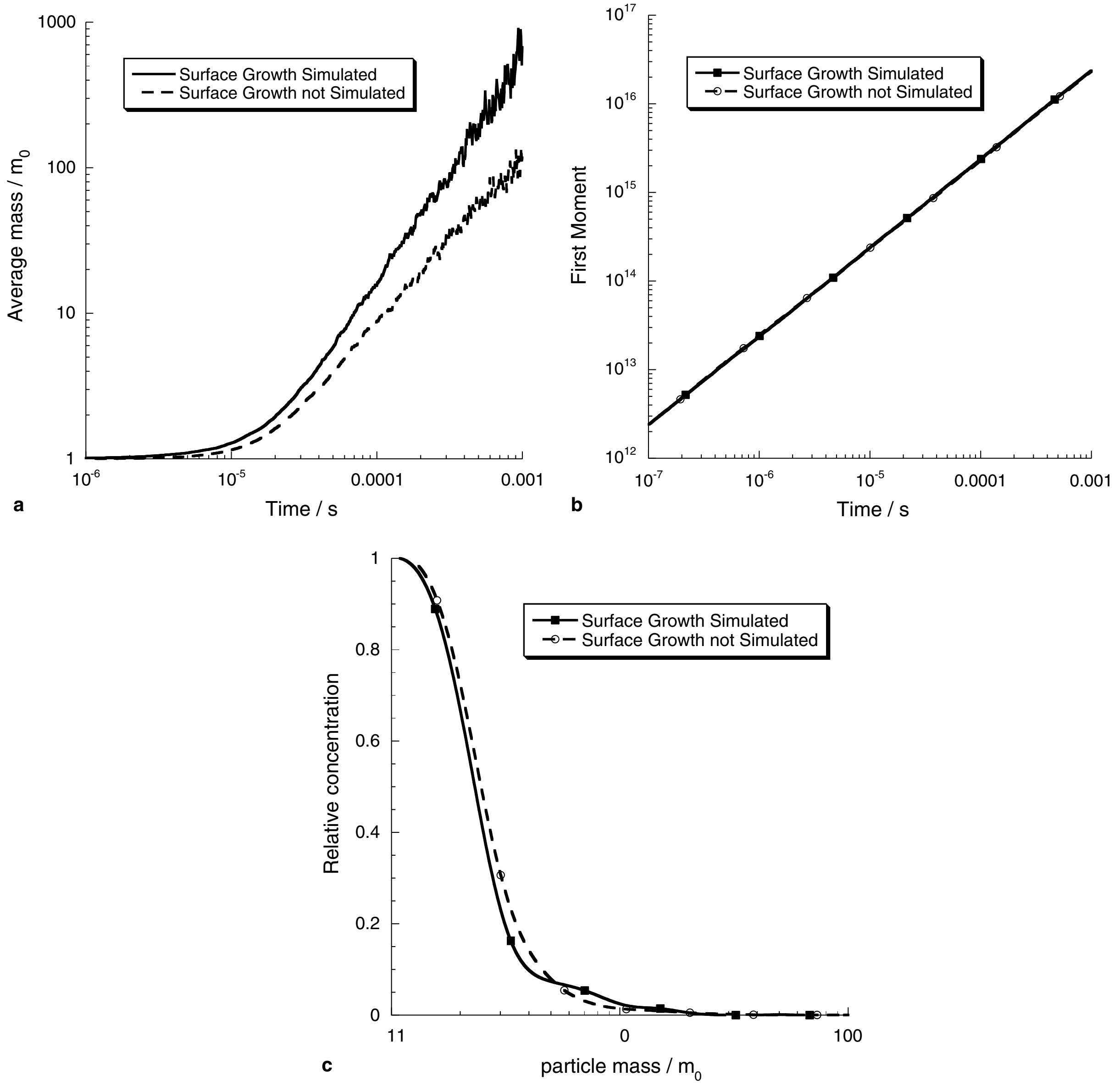

Fig. 8. (a) Average mass vs time. (b) First moment vs time. (c) PSD of TiO_2 size at $t = 0.001$ s. Various properties of TiO_2 system with and without surface growth simulated.

7. Conclusions

In this paper we have shown how a model for nanoparticle growth may be transformed into a vague form and generators of a stochastic process are deduced. This led us to derive a new mass-flow algorithm, which can be applied to the simulation of coagulation, particle source and surface-growth processes.

A numerical implementation of the algorithm was used to simulate a test situation for which various convergence properties could be calculated. The CPU time that the algorithm ran in was found to scale linearly with the normalization parameter, N, whilst the total errors in average size and second and third moments were found to decrease as $1/\sqrt{N}$. For small N, when the systematic errors dominate the solution, the error was found to decrease linearly in N. The total error in the solution for these simulations was two orders of magnitude less than when compared to the similar direct simulation algorithm.

Three particle systems were simulated using the mass flow algorithm. The silica system was simulated for increasing initial concentrations of the precursor SiH_4, with the results calculated being in good agreement with the experimental data obtained from the literature.

The formation of iron oxide was also simulated under varying initial concentrations of the precursor. At low concentrations, the results were in very good agreement with the experimental data obtained from the literature. At higher concentrations however, the difference between the model and the experiments differed greatly. This has been attributed to a lack of kinetic data for the oxidation of $FeCO_5$.

Finally, a simple titania system was simulated for both high and low initial concentrations of $TiCl_4$. The systems were simulated both with and without surface growth. It was found that surface growth is most important for high initial concentrations of $TiCl_4$ which is in accordance with [20].

Acknowledgments

The authors thank the EPSRC (Grant No. GR/R85662/01) for the financial support of N.M.M. and W.W. under the title 'Mathematical and Numerical Analysis of Coagulation-Diffusion Processes in Chemical Engineering' and the Oppenheimer Fund for the support of C.G.W. The authors thank one of the reviewers of this paper for their helpful comments.

References

[1] M. Frenklash, S. Harris, Aerosol dynamics modelling using the method of moments, J. Colloid Interf. Sci. 118 (1) (1986) 252–262.

[2] M.J. Hounslow, A discretised population balance for continuous systems at steady state, AIChE J. 36 (1) (1990) 106–116.

[3] M.K. Akhtar, G.G. Lipscombe, S.E. Pratsinis, Monte Carlo simulation of particle coagulation and sintering, Aerosol Sci. Technol. 21 (1) (1994) 83–93.

[4] P. Tandon, D.E. Rosner, Monte Carlo simulation of particle aggregation and simultaneous restructuring, J. Colloid Interf. Sci. 213 (1999) 273–286.

[5] D. Grosschmidt, H. Bockhorn, M. Goodson, M. Kraft, Two approaches to the simulation of silica particle systems, Proc. Combust. Inst. 29 (2002) 1039–1046.

[6] C.G. Wells, M. Kraft, Direct simulation and mass flow stochastic algorithms to solve a sintering-coagulation equation, Monte Carlo Meth. Appl. 11 (2) (2005) 175–198.

[7] D.T. Gillespie, The stochastic coalescence model for cloud droplet growth, J. Atmos. Sci. 29 (1972) 1496–1510.

[8] A. Eibeck, W. Wagner, Approximate solution of the coagulation-fragmentation equation by stochastic particle systems, Stoch. Anal. Appl. 18 (2000) 921–948.

[9] A. Eibeck, W. Wagner, An efficient stochastic algorithm for studying coagulation dynamics and gelation phenomena, SIAM J. Sci. Comput. 22 (2000) 802–821.

[10] A. Eibeck, W. Wagner, Stochastic particle approximations for Smoluchowski's coagulation equation, Ann. Appl. Probab. 11 (2001) 1137–1165.

[11] A. Kolodko, K. Sabelfeld, Stochastic particle methods for Smoluchowski coagulation equation: variance reduction and error estimations, Monte Carlo Meth. Appl. 9 (4) (2004) 315–339.

[12] A.H. Marcus, Stochastic coalescence, Technometrics 10 (1968) 133–148.

[13] A.A. Lushnikov, Some new aspects of coagulation theory, Izv. Akad. Nauk. SSSR Ser. Fiz Atmosfer. i Okeana 14 (1978) 738–743.

[14] M. Goodson, M. Kraft, An efficient algorithm for simulating nano-particle dynamics, J. Comput. Phys. 183 (2002) 210–232.

[15] E. Debry, B. Sportisse, B. Jourdain, A stochastic approach for the numerical simulation of the general dynamics equation for aerosols, J. Comput. Phys. 184 (2003) 649–669.

[16] H. Babovsky, On a Monte Carlo scheme for Smoluchowski's coagulation equation, Monte Carlo Meth. Appl. 5 (1) (1999) 1–18.

[17] N. Peters, J. Warnatz (Eds.), Numerical methods in laminar flame propagation: A GAMM-Workshop. Braunschweig, Vieweg, 1982.

[18] J. Kee, K. Grcar, M.D. Smooke, J.A. Miller, PREMIX: A FORTRAN program for modelling steady laminar one-dimensional premixed flames, Technical report, SANDIA National Laboratories, 1985.

[19] M. von Smoluchowski, Drei Vorträge über Diffusion, Brownsche Molekularbewegung und Koagulation von Kolloidteilchen, Phys. Z. 17 (1916) 557–571, 585–599.

[20] P.T. Spicer, O. Chaoul, S. Tsantilis, S.E. Pratsinis, Titania formation by $TiCl_4$ gas phase oxidation, surface growth and coagulation, J. Aerosol Sci. 33 (2002) 17–34.

[21] S.E. Pratsinis, H. Bai, P. Biswas, M. Frenklach, S.V.R. Mastrangelo, Kinetics of $TiCl_4$ oxidation, J. Am. Ceram. Soc. 73 (1990) 2158–2162.

[22] B.B. Mandelbrot, The Fractal Geometry of Nature, Freeman, San Francisco, CA, 1982.

[23] M. Kraft, W. Wagner, Numerical study of a stochastic particle method for homogeneous gas phase reactions, Comput. Math. Appl. 45 (2003) 329–349.

[24] D. Lindackers, M.G.D. Strecker, P. Roth, C. Janzen, S.E. Pratsinis, Formation and growth of SiO_2 particles in low pressure H_2/O_2/Ar flames doped with SiH_4, Combust. Sci. Technol. 123 (1997) 287–315.

[25] R.J. Kee, F.M. Rupley, E. Meeks, J.A. Miller, CHEMKIN-III: A FORTRAN chemical kinetics package for the analysis of gas-phase chemical and plasma kinetics, Technical report, 1996.

[26] R.J. Kee, G. Dixon-Lewis, J. Warnatz, M.E. Coltrin, J.A. Miller, A FORTRAN computer code package for the evaluation of gas-phase multicomponent transport properites. Technical report, SANDIA National Laboratories, 1992.

[27] C. Janzen, P. Roth, Formation and characteristics of Fe_2O_3 nano-particles in doped low pressure H_2/O_2/Ar flames, Combust. Flame 125 (2001) 1150–1161.

[28] A. Giesen, J. Herzler, P. Roth, Kinetics of Fe-atom condensation based on Fe-condensation measurement, J. Phys. Chem. A 107 (26) (2003) 5202–5207.

[29] A. Giesen, D. Woiki, J. Herzler, P. Roth, Oxidation of Fe atoms by O_2 based on Fe- and O- concentration measurements, Proc. Combust. Inst. 29 (Part 1) (2002) 1345–1352.

[30] NIST website. http://webbook.nist.gov/chemistry.